Article:
Brandolini, N, Kapur, N and Hall, RM (2014) Dynamics of interpedicular widening in spinal burst fractures: an in vitro investigation. Spine Journal, 14 (9). pp. 2164-2171. ISSN 1529-9430

https://doi.org/10.1016/j.spinee.2014.01.058

Elsevier Editorial System(tm) for The Spine Journal
Manuscript Draft

Manuscript Number: SPINEE-D-13-00843R1

Title: Dynamics of interpedicular widening in spinal burst fractures: an in vitro investigation.

Article Type: Basic Science

Section/Category: Biomechanics

Keywords: In vitro biomechanics of the spine; dynamics of spinal burst fracture; dynamic interpedicular widening; canal occlusion.

Corresponding Author: Mr. Nicola Brandolini,

Corresponding Author's Institution: School of Mechanical Engineering

First Author: Nicola Brandolini

Order of Authors: Nicola Brandolini; Nikil Kapur, PhD; Richard M Hall, PhD

Abstract: BACKGROUND CONTEXT: Spinal burst fractures are a significant cause of spinal instability as well as neurological impairment. Whilst evidence suggests that the neurological trauma arises during the dynamic phase of fracture, the biomechanics underpinning the phenomenon has yet to be fully explained. Interpedicular widening (IPW) is a distinctive feature of the fracture but, despite the association with the occurrence of neurological deficit, little is known about its biomechanics.
PURPOSE: To provide a comprehensive in vitro study on spinal burst fracture, with special attention on the dynamics of IPW.
STUDY DESIGN: Experimental measurements in combination with CT scanning were used to quantitatively investigate the biomechanics of burst fracture in a cadaveric model.
METHODS: Twelve human three-adjacent-vertebrae segments were tested to induce burst fracture. Impact was delivered through a drop weight tower whilst IPW was continuously recorded by two displacement transducers. CT scanning aided quantifying canal occlusion as well as evaluating sample anatomy and fracture appearance. Two levels of energy were delivered to two groups: high (HE) and low (LE). This study was funded by the EU within the project SPINEFX-ITN (grant agreement no. PITN-GA-2009-238690-SPINEFX).
RESULTS: No difference was found between HE and LE in terms of the residual IPW (i.e. post-fracture), maximum IPW, or canal occlusion (median 20.2%). Whilst IPW was not found to be correlated with canal occlusion, a moderate correlation was found between the maximum and the residual IPW. At the fracture onset, IPW reached a maximum median value of 15.8% in ~20-25 ms. Following the transient phase, the pedicles were recoiled to a median residual IPW of 4.9%.
CONCLUSIONS: Our study provides for the first time insight on how IPW actually evolves during the fracture onset. In addition, our results may help shedding more light in the mechanical initiation of the fracture.

Dynamics of interpedicular widening in spinal burst fractures: an *in vitro* investigation.

Nicola Brandolini, M.Sc. [1], Nikil Kapur, Ph.D. [1], Richard M. Hall, Ph.D. [1]

[1] School of Mechanical Engineering, University of Leeds, Leeds, UK

Corresponding author:
Nicola Brandolini
Institute of Medical and Biological Engineering – School of Mechanical Engineering
University of Leeds
Woodhouse Lane
LS2 9JT, LEEDS, UK
tel: +44-1133439408
e-mail: n.brandolini@leeds.ac.uk

ABSTRACT

BACKGROUND CONTEXT: Spinal burst fractures are a significant cause of spinal instability as well as neurological impairment. Whilst evidence suggests that the neurological trauma arises during the dynamic phase of fracture, the biomechanics underpinning the phenomenon has yet to be fully explained. Interpedicular widening (IPW) is a distinctive feature of the fracture but, despite the association with the occurrence of neurological deficit, little is known about its biomechanics.

PURPOSE: To provide a comprehensive in vitro study on spinal burst fracture, with special attention on the dynamics of IPW.

STUDY DESIGN: Experimental measurements in combination with CT scanning were used to quantitatively investigate the biomechanics of burst fracture in a cadaveric model.

METHODS: Twelve human three-adjacent-vertebrae segments were tested to induce burst fracture. Impact was delivered through a drop weight tower whilst IPW was continuously recorded by two displacement transducers. CT scanning aided quantifying canal occlusion as well as evaluating sample anatomy and fracture appearance. Two levels of energy were delivered to two groups: high (HE) and low (LE). This study was funded by the EU within the project SPINEFX-ITN (grant agreement no. PITN-GA-2009-238690-SPINEFX).

RESULTS: No difference was found between HE and LE in terms of the residual IPW (i.e. post-fracture), maximum IPW, or canal occlusion (median 20.2%). Whilst IPW was not found to be correlated with canal occlusion, a moderate correlation was found between the maximum and the residual IPW. At the fracture onset, IPW reached a maximum median value of 15.8% in ~20-25 ms. Following the transient phase, the pedicles were recoiled to a median residual IPW of 4.9%.

CONCLUSIONS: Our study provides for the first time insight on how IPW actually evolves during the fracture onset. In addition, our results may help shedding more light in the mechanical initiation of the fracture.

1. INTRODUCTION

Burst fractures account for about 30% of all spinal injuries [1] and are a cause of severe neurologic impairment as well as spinal instability [2]. Approximately 47% of cases present with a degree of neurological deficit at the time of admission [3].

The onset of the fracture is usually traumatic and arises from a high-energy axial impact loading, commonly due to fall by heights and motor accidents [4]. The main features of the fracture are comminution of the endplates, loss of vertebral height, disruption of the posterior ligamentous complex, retropulsion of bony fragment into the spinal canal (FR), laminar fracture (LF) and widening of the interpedicular distance [1, 3, 5].

Canal occlusion caused by FR has been shown to be a significant risk factor of neurological deficit [6]. However, canal occlusion alone appears not to fully explain the extent of the neurologic deficit [3, 7]. Further additional insight into the generation of burst fractures can be accrued from the fact that neurologic deficit has been diagnosed in 68% of the patients with disruption of the posterior elements [8] whilst dural tears have been detected in 25% of low lumbar burst fractures [9] and their occurrence has been shown to be strongly associated with interpedicular widening and LFs [10, 11].

The clinical relevance of interpedicular widening has been also confirmed by [12], where a ~25% widening has been found to be associated with a 51% probability of presenting neurologic deficit. Ultimately, assessment of post-traumatic interpedicular widening may provide a more time and cost effective diagnostics since it can be better quantified on plain radiographs than spinal occlusion [13].

However, the real drawback in the diagnosis of any burst fracture caused impairment is that the actual injury originates during an extremely abrupt transient phase that cannot be quantified retrospectively. Hence, the need for more understanding on the dynamic

biomechanics of burst fracture is paramount. Several in vitro studies have indeed shown that the maximum canal occlusion occurs during the onset of the fracture [14-18].

In addition, further biomechanical studies have suggested that the root of the pedicles is the site of initiation of burst fracture. Both in vitro [19] and numerical simulations [20] have detected significant strain concentration at the base of the pedicles. In [21] the fracture initiation process has been demonstrated to be driven by the forces that originate at the pedicles when the superior facets wedge within their own adjacent joints. Unlike the dynamics of canal occlusion, which has been the subject of several biomechanical studies, interpedicular widening has not been investigated in a manner that would provide a greater understanding of the fracture process and aid its use in clinical diagnoses.

Therefore, the aim of this work was to investigate, for the first time, the dynamics underlying the behavior of the facet joints and pedicles during the generation of a spinal burst fracture. In addition, high resolution peripheral quantitative computed tomography (HR-pQCT) was exploited to provide a comprehensive view of the phenomena, pre- and post-fracture.

2. MATERIALS AND METHODS

2.1. Specimen preparation

Four human spines were acquired following ethics committee approval from the Leeds Tissue Bank (Leeds Teaching Hospitals Trust, Leeds, UK). Three, three-adjacent-vertebrae segments (T9-T10-T11, T12-L1-L2 and L3-L4-L5) were harvested from each spine for a total of 12 specimens (Table 1). Care was taken to preserve the intervertebral discs, the principal ligamentous structures and the integrity of the superior and inferior facet joints adjacent to the central vertebra. No alterations were performed to any of the vertebra to force the occurrence and appearance of a burst fracture.

The cranial and caudal vertebrae of each segment were partially embedded in polymethyl methacrylate (PMMA, WHW Plastics, Hull, UK) to provide two flat parallel loading surfaces as well as consistently align the specimen within the testing rig. To this end, a stainless steel rod was firmly clamped against the posterior wall of the most distal vertebrae to firmly hold the sample in place whilst being embedded. The location of the rod within the canal was adjusted to make the superior and inferior rim of the central vertebral body as parallel to the ground as possible. The most anterior region of the central vertebra and its spinous process were used as references to define the sagittal plane of the segment which was aligned with the center lines of the potting molds.

2.2. Experimental protocol

A custom testing rig was designed to fit within a drop weight tower (Fig. 1). Hence, in order to simulate an axial impact load, a weight was dropped down a guide rod against the upper surface of an impactor. This technique was previously verified and successfully exploited on animal tissue within the same institute as the authors' [18, 22]. The lower extremity of the specimen was secured in a fixed stainless steel pot whilst the upper extremity was positioned under the lower surface of the impactor. The impactor resting on the specimen resulted in a preload of approximately 50 N.

Specimens were divided in two groups (two T10, two L1 and two L4 per group) to be evenly distributed in BMD ($p=0.59$) as well as anatomically (for what concerned the measurements performed). In fact, no differences were found between the two groups regarding the initial interpedicular distance ($p=0.63$), the initial spinal canal area ($p=0.94$) and the pedicle angles ($p=0.67$), which increased in the caudal direction ($p=0.0098$).

Each group underwent two different level of energy to simulate a high (HE) and a lower (LE) energy impact. The energy delivered to each specimen was tuned according to the bone

volumetric mass density (BMD) and minimum cross sectional area (CSA_{min}) of the central vertebra of each specimen. Following a set of initial experiments, LE was identified as an approximate lower value of energy needed to induce a spinal burst fracture in each specimen. Likewise, HE was defined to be a 20% increase with respect to LE. Samples were kept wrapped in moist tissues during tests to keep the tissue hydrated.

Interpedicular widening was calculated from the measurements of two linear displacement transducers (LVDT, type ACT1000A, RDP Electronics, Wolverhampton, UK). Each LVDT was sampled continuously at 5000 Hz for one second during the impact with the recordings set off by an optical trigger (W250 series, SICK, Waldkirch, Germany). Both the LVDTs and trigger were connected to a data acquisition board (NI cRIO-9074 equipped with NI 9215 module, National Instruments Corporation, Austin, Texas, USA chassis). Data logging and signal manipulation were performed through a custom made code (LabVIEW 2011 SP1, National Instruments Corporation, Austin, TX, USA).

Location of each LVDT was chosen on each specimen to ensure contact of the LVDT tip against a reproducible measurement point. Where the central vertebra was lumbar (L1, L4), a flat dish-shaped tip was mounted onto the stem of the LVDTs and put in contact with the most lateral region of the superior facet joints. The initial interpedicular distance (l_0) was defined as the distance between the measuring plates (Fig. 1). Where the central vertebra was thoracic (T10), a spherical tip was fastened onto the stem and put in contact with the region posteriorly to the root of the pedicles (the exact location was adjusted depending on the features of the bony surface). In addition, l_{0CT} was estimated from HR-pQCT (XtremeCT, Scanco Medical, Brüttisellen, Switzerland) scans by matching anatomical features identified on the specimens. This measurement location was chosen as the thoracic vertebrae do not have interlocking facet joints that protrude laterally from the pedicles as in the lumbar spine. In all cases, the LVDTs were aligned to keep the measuring direction parallel to the frontal

plane and perpendicular to the loading axis (Δl_{RIGHT} and Δl_{LEFT} were respectively the displacements measured by the right and left LVDTs). Therefore, the percent interpedicular widening (IPW) was calculated as follow (with l_{0CT} in T10):

$$IPW = \frac{\Delta l_{RIGHT} + \Delta l_{LEFT}}{l_0} 100$$

The following quantities were identified on each IPW curve:

- IPW_{max}: The maximum percent interpedicular widening was identified as the maximum value assumed by the IPW during the impact.
- IPW_{res}: The residual percent interpedicular widening was identified as the residual value assumed by the IPW at the end of the dynamic phase.

2.3. HR-pQCT scanning

Each specimen (whole three-adjacent-vertebrae segment) was scanned on HR-pQCT prior and after testing using an isotropic voxel size of 82 μm. Scans were used to calculate the following parameters on the central vertebra of each specimen using an image processing software [23].

- BMD: calculated over a cylindrical volume centered at 40% of antero-posterior distance (AP), with diameter of 60% AP and height of 80% of the total vertebral height, as in [24].
- Pedicle angle (PA): defined as the angle between the direction of the root of the pedicle and the AP direction, as in [25].
- Canal occlusion (CO): the minimum area within the spinal canal area prior to test (CA_0) and after (CA_1) was manually outlined on the slices of interest. Therefore, CO was calculated as in [8, 17]:

$$CO = \frac{(CA_0 - CA_1)}{CA_0} 100$$

- Interpedicular widening (IPW_{CT}): the post-fracture interpedicular distance (l_{1CT}) was estimated by matching the measurement locations of the LVDTs on the CT slices and compared to l_0 (or l_{0CT} in T10).

$$IPW_{CT} = \frac{(l_{1CT} - l_0)}{l_0} 100$$

Images from the scans were also used to identify the presence of LF, FR and grade the fracture type in accordance with [1].

2.4. Statistical analysis

Because of the limited sample size non parametric statistics was performed. Differences among results were assessed using Mann-Whitney U test and Kruskal-Wallis one-way analysis of variance by ranks. Association between variables was assessed using the Spearman's rank correlation coefficient (r_s). In all cases, a nominal significance level of 0.05 was used. Agreement was analyzed using the technique outlined by [26].

All statistical analyses were performed using designated software (R v. 3.0.1, R Foundation for Statistical Computing, Vienna, Austria).

3. RESULTS

Burst fractures were induced in all the specimens (Fig. 2) and the injury at the central vertebra was graded (Tab. 2). Fractures of the pedicles of various severities were detected in all the specimens at the level of the central vertebra. In the specimen L3-L4-L5 from donor A the fracture occurred on L4 was of type B2.3.1 (i.e. fracture of the pedicles associated with

compression fracture) with comminution of L5's cranial endplate. In all the other specimens a burst fracture (type A3, different subtypes) always occurred at the level of the central vertebra.

The median energy delivered to each group was 200.3 J (HE, range: 166.2-223.8 J) and 157.6 J (LE, range: 146.0-184.2 J). Since the drop height was kept as constant as possible (overall median: 1.46 m), the overall median velocity at the impact was estimated to be 5.35 m/s (no difference between groups, p=0.37).

The median CO in the HE group was 32.4 % (range: 9.7-41.2 %) and 11.8 % (range: -9.0-51.5 %) in the LE group. No difference was found between the two groups (p=0.13) or amongst the three spinal levels (p=0.23). A moderate correlation (r_s=0.56, p=0.063) was found between CO and the amount of energy delivered (Fig. 3).

Agreement between measurements of residual IPW through the LVDTs (IPW_{res}) and HR-pQCT scans (IPW_{CT}) was found to be about ±3% (95% agreement interval). However, it was not possible to calculate IPW_{res} in two samples as the LVDTs lost contact of the bony surface after the transient phase of the impact.

Overall trend of the IPW curves is presented in Fig. 4. The time elapsed between the beginning of the displacement and IPW_{max} was estimated to be ~20-25 ms whilst the whole transient phase lasted ~400 ms.

The median IPW_{max} and IPWres were 11.0% (range: 4.3-40.7%) and 1.7 % (range: -0.3-10.2 %) for the HE group and 17.3% (range: 6.9-21.8%) and 7.0 % (range: -1.3-11.5 %) for the LE group, respectively. However, no difference was found between the two groups (Fig. 5) for both IPW_{max} (p=0.70) and IPW_{res} (p=0.84). IPW_{max} was significantly higher than IPW_{res} (p=0.011) and the two quantities showed a moderate correlation between each other (r_s=0.58, p=0.088). No correlation was found between IPW and the delivered energy (IPW_{max}: r_s=-0.29, p=0.37; IPW_{res}: r_s=-0.14, p=0.71) as well as between IPW and CO (IPW_{max}: r_s=0.042,

p=0.90; IPW_{res}: r_s=-0.24, p=0.50). The level to which the central vertebra belonged marginally influenced both IPW_{max} (p=0.077) and IPW_{res} (p=0.055) (Fig. 6).

When the maximum interpedicular displacement was considered in its absolute values (maximum value of Δl_{RIGHT} and Δl_{LEFT}) no difference was again found between the HE and LE group (p=0.84). On the other hand, a significant difference was found among levels (p=0.022). In particular, a significant difference was found between T10 and L4 (p=0.038) as well as L1 and L4 (p=0.0070). The maximum absolute interpedicular displacement did not show any correlation with the pedicle angle (r_s=-0.14, p=0.51).

LF were detected in seven specimens whilst FR in eight, presence of LF was always associated with FR, resulting in higher extent of median CO (p=0.048).

4. DISCUSSION

Increase of the interpedicular distance, splaying of the facet joints and LF are peculiar features of the spinal burst fracture [3] and their association with neurologic deficit and dural tears has been shown in several clinical studies [10, 12]. It is however during the transient and abrupt onset of the fracture that the actual neurological injury occurs [27]. Hence, a thorough understanding of the dynamics of the fracture may yield to more valid diagnostics and treatment definition.

Several in vitro studies have shown how canal occlusion reaches its peak value during the dynamic stage of the fracture. The same mechanism may apply to interpedicular widening; notwithstanding, no works have ever corroborated this hypothesis nor provided any dynamic measurement. In our study we found that, during the development of the fracture, IPW reached a maximum value significantly higher than at the post-fracture evaluation. In fact, IPW_{max} showed a 223% increase with respect to IPW_{res} whilst only moderate correlation was found between them. Although Panjabi et al. [27] have reported the maximum dynamic canal

occlusion to be 85% more than the static measurement, neither Panjabi et al. [27] nor Wilcox et al. [18] have found any correlation between the maximum and the residual occlusion, an indication that the dynamic canal occlusion alone may not be enough to understand the origin of the trauma.

Although a moderate correlation has been found in vivo between interpedicular widening and CO [28], we did not find any correlation between both IPW_{max}, IPW_{CT} and CO. On the other hand, a moderate correlation was found between CO and the energy, as well as between IPW_{max} and IPW_{res}.

Repeatability is generally a disputable issue when in vitro burst fractures are to be reproduced, with experimental fracture patterns seldom matching what seen in vivo [21]. However, the values of CO obtained in this study (median 20.2%) were comparable to what obtained in other in vitro studies (e.g. Jones et al. [29] induced 30% average CO) whilst the fractures' aspect overall matched what seen clinically [1, 3]. In addition, the duration of the initial dynamic phase as simulated in our study was comparable to what reported by Ivancic [30]. In his work, the occurrence of burst fracture due to a fall from height was simulated in vitro by fitting a spine segment into an instrumented dummy whose transducers recorded major transient events up to ~70 ms.

An average IPW of 24.7% has been found in vivo in presence of neurologic deficit and 15.3% in its absence [12]. In our study the median IPW_{CT} was 4.7%, which may be representative of less severe fractures. However, our study lacked of any muscle simulation. Although in vivo IPW have been shown not to be affected when either supine or erect radiographs are taken [31], the pressure from adjacent tissues, as well as paraspinal muscular contraction may have resulted in higher IPW in vivo. Furthermore, Caffaro and Avanzi [12], have found an increasing trend in IPW in caudal direction whilst we only observed a marginal variation in

IPW_{CT} among levels. This might be because of the in vitro setting itself, which provides more controlled loading conditions whilst lacking the biomechanics of the rest of the body.

Several biomechanical studies have postulated that the posterior articular processes as the initiator of the burst fracture and our study provided further insight into the dynamics of the trauma. In fact, surface strain measurements have shown the root of the pedicle as a major site of strain concentration under axial loading conditions [19]. Numerical simulations by Wilcox et al. [20] have reported a significant tensile strain concentration in the posterior region of the vertebral body originating from the facet joints. Langrana et al. [21] reviewed the loading mechanism of burst fractures providing evidences that the fracture originates from a complex loading condition made of: i) axial loading through the endplates; ii) splaying forces at the root of the pedicles induced by the forceful downward displacement of the adjacent facets. Results obtained in our study added further insight into the dynamics of burst fractures. In fact, the IPW curves (Fig. 4) may confirm that the widening is driven by the wedging effect of the superior facets, regardless of whether we had HE or LE conditions. Hence, the mentioned wedging effect may have induced the initial rapid displacement which culminated into the failure of the pedicles when the critical displacement peak was reached (IPW_{max}). The orientation of the pedicle did not influence the dynamics of IPW, although a significant difference was found among the levels for IPW_{max}. Following the initial dynamic phase, the pedicles were recoiled to their final position (IPW_{res}, IPW_{CT}).

Despite the consistent results and injury patterns induced in the samples, the authors are aware that the fractures induced on T10 levels may not be fully representative of the in vivo conditions as the stiffening effect of the rib cage was missing. Furthermore, T10's anatomy required the LVDTs to be positioned differently from the other samples, which may have influenced the related results.

Some might question our choice of using spring loaded LVDTs to measure such a dynamic event as the force exerted by the spring itself (nominally 2 N) may have constrained the displacement of the bony region. However, this effect was neglected as a power of ~1.24 W was estimated to be required to reach the maximum widening (12.4 mm) in 20 ms.

In their study, Hashimoto et al. [8] found an association between canal shape and neurologic deficit. Vaccaro et al. [32] has also indicated the shape of the canal, rather than its residual area, as a risk factor for spinal cord injury. Therefore, it is plausible to assume that the neurological trauma may arise from a combination of dynamic IPW and posterior wall deformation.

The origination of dural tears may also be strictly related to IPW. In their retrospective study on burst fracture patients, Cammisa et al. [33] found a significant association between LFs and dural tears, also finding entrapment of neurological elements between the fracture edges. They theorized that a splay of the pedicles at the fracture onset would result in the LF reaching a maximum width too. Retropulsion of bone fragments would then make the dura mater protrude through the fracture edge, hence remaining entrapped (i.e. lacerating the dural sac) when the pedicles are recoiled to their resting position. To the authors' knowledge, our study provided for the first time quantitative evidence of this phenomenon. However, a similar investigation on the dynamics of LF would definitely help shedding more light on the etiology of dural tears.

In conclusion, the integration of our results with other studies on dynamic CO (and potentially LF) may allow implementing novel clinical tools to estimate retrospectively the evolution of the spinal canal during the fracture, hence aiding assessment of the neurological deficit (also predicting the risk of dural tears) as well as design of the optimal treatment.

References

[1] Magerl F, Aebi M, Gertzbein SD, Harms J, Nazarian S. A comprehensive classification of thoracic and lumbar injuries. Eur Spine J. 1994;3(4):184-201.

[2] Petersilge CA, Emery SE. Thoracolumbar burst fracture: evaluating stability. Semin Ultrasound CT MR. 1996;17(2):105-13.

[3] Denis F. The three column spine and its significance in the classification of acute thoracolumbar spinal injuries. Spine (Phila Pa 1976). 1983;8(8):817-31.

[4] Meves R, Avanzi O. Correlation among canal compromise, neurologic deficit, and injury severity in thoracolumbar burst fractures. Spine (Phila Pa 1976). 2006;31(18):2137-41.

[5] Saifuddin A, Noordeen H, Taylor BA, Bayley I. The role of imaging in the diagnosis and management of thoracolumbar burst fractures: current concepts and a review of the literature. Skeletal Radiol. 1996;25(7):603-13.

[6] Yugue I, Aono K, Shiba K, et al. Analysis of the risk factors for severity of neurologic status in 216 patients with thoracolumbar and lumbar burst fractures. Spine (Phila Pa 1976). 2011;36(19):1563-9.

[7] Park JK, Park JW, Cho DC, Sung JK. Predictable factors for dural tears in lumbar burst fractures with vertical laminar fractures. J Korean Neurosurg Soc. 2011;50(1):11-6.

[8] Hashimoto T, Kaneda K, Abumi K. Relationship between traumatic spinal canal stenosis and neurologic deficits in thoracolumbar burst fractures. Spine (Phila Pa 1976). 1988;13(11):1268-72.

[9] Ozturk C, Ersozlu S, Aydinli U. Importance of greenstick lamina fractures in low lumbar burst fractures. Int Orthop. 2006;30(4):295-8.

[10] Lee IS, Kim HJ, Lee JS, et al. Dural tears in spinal burst fractures: predictable MR imaging findings. AJNR Am J Neuroradiol. 2009;30(1):142-6.

[11] Tisot RA, Avanzi O. Laminar fractures as a severity marker in burst fractures of the thoracolumbar spine. J Orthop Surg (Hong Kong). 2009;17(3):261-4.

[12] Caffaro MF, Avanzi O. Can the interpedicular distance reliably assess the severity of thoracolumbar burst fractures? Spine (Phila Pa 1976). 2012;37(4):E231-6.

[13] Bensch FV, Koivikko MP, Kiuru MJ, Koskinen SK. Measurement of spinal canal narrowing, interpedicular widening, and vertebral compression in spinal burst fractures: plain radiographs versus multidetector computed tomography. Skeletal Radiol. 2009;38(9):887-93.

[14] Tran NT, Watson NA, Tencer AF, Ching RP, Anderson PA. Mechanism of the burst fracture in the thoracolumbar spine. The effect of loading rate. Spine (Phila Pa 1976). 1995;20(18):1984-8.

[15] Kifune M, Panjabi MM, Liu W, Arand M, Vasavada A, Oxland T. Functional Morphology of the Spinal Canal After Endplate, Wedge, and Burst Fractures. Journal of Spinal Disorders & Techniques. 1997;10(6):457-66.

[16] Carter JW, Mirza SK, Tencer AF, Ching RP. Canal geometry changes associated with axial compressive cervical spine fracture. Spine (Phila Pa 1976). 2000;25(1):46-54.

[17] Panjabi MM, Hoffman H, Kato Y, Cholewicki J. Superiority of incremental trauma approach in experimental burst fracture studies. Clin Biomech (Bristol, Avon). 2000;15(2):73-8.

[18] Wilcox RK, Boerger TO, Allen DJ, et al. A dynamic study of thoracolumbar burst fractures. J Bone Joint Surg Am. 2003;85-A(11):2184-9.

[19] Hongo M, Abe E, Shimada Y, Murai H, Ishikawa N, Sato K. Surface strain distribution on thoracic and lumbar vertebrae under axial compression. The role in burst fractures. Spine (Phila Pa 1976). 1999;24(12):1197-202.

[20] Wilcox RK, Allen DJ, Hall RM, Limb D, Barton DC, Dickson RA. A dynamic investigation of the burst fracture process using a combined experimental and finite element approach. Eur Spine J. 2004;13(6):481-8.

[21] Langrana NA, Harten RR, Lin DC, Reiter MF, Lee CK. Acute thoracolumbar burst fractures: a new view of loading mechanisms. Spine (Phila Pa 1976). 2002;27(5):498-508.

[22] Tarsuslugil SM, O'Hara RM, Dunne NJ, et al. Development of calcium phosphate cement for the augmentation of traumatically fractured porcine specimens using vertebroplasty. J Biomech. 2013;46(4):711-5.

[23] Schneider CA, Rasband WS, Eliceiri KW. NIH Image to ImageJ: 25 years of image analysis. Nat Methods. 2012;9(7):671-5.

[24] Furtado N, Oakland RJ, Wilcox RK, Hall RM. A biomechanical investigation of vertebroplasty in osteoporotic compression fractures and in prophylactic vertebral reinforcement. Spine (Phila Pa 1976). 2007;32(17):E480-7.

[25] Zindrick MR, Wiltse LL, Doornik A, et al. Analysis of the morphometric characteristics of the thoracic and lumbar pedicles. Spine (Phila Pa 1976). 1987;12(2):160-6.

[26] Bland JM, Altman DG. Statistical methods for assessing agreement between two methods of clinical measurement. Lancet. 1986;1(8476):307-10.

[27] Panjabi MM, Kifune M, Wen L, et al. Dynamic canal encroachment during thoracolumbar burst fractures. J Spinal Disord. 1995;8(1):39-48.

[28] Mumford J, Weinstein JN, Spratt KF, Goel VK. Thoracolumbar burst fractures. The clinical efficacy and outcome of nonoperative management. Spine (Phila Pa 1976). 1993;18(8):955-70.

[29] Jones HL, Crawley AL, Noble PC, Schoenfeld AJ, Weiner BK. A novel method for the reproducible production of thoracolumbar burst fractures in human cadaveric specimens. Spine J. 2011;11(5):447-51.

[30] Ivancic PC. Hybrid cadaveric/surrogate model of thoracolumbar spine injury due to simulated fall from height. Accid Anal Prev. 2013;59C:185-91.

[31] Mehta JS, Reed MR, McVie JL, Sanderson PL. Weight-bearing radiographs in thoracolumbar fractures: do they influence management? Spine (Phila Pa 1976). 2004;29(5):564-7.

[32] Vaccaro AR, Nachwalter RS, Klein GR, Sewards JM, Albert TJ, Garfin SR. The significance of thoracolumbar spinal canal size in spinal cord injury patients. Spine (Phila Pa 1976). 2001;26(4):371-6.

[33] Cammisa FP, Jr., Eismont FJ, Green BA. Dural laceration occurring with burst fractures and associated laminar fractures. J Bone Joint Surg Am. 1989;71(7):1044-52.

Figure Captions

Fig. 1 – Pictorial representation of the testing rig. a) sample; b) LVDT (recordings were set off by an optical trigger sampled at 5000 Hz whilst in await for the dropped weight to cross its light path); c) impactor; d) impactor shaft housing: a ball bushing allowed minimizing any loss of kinetic energy due to friction.

Fig. 2 – 3D representation obtained from the post-fracture HR-pQCT scan of a T12-L1-L2 specimen. Complete burst fracture was induced only on L1 (graded as A3.3.3), leaving the adjacent vertebrae intact. Main features of the fracture can be identified: a) comminution of the endplate; b) fragment retropulsion into the spinal canal; b) laminar fracture; d) pedicular failure (i.e. resulting in interpedicular widening).

Fig. 3 – Percent canal occlusion (CO) divided by group (HE and LE) plotted with respect to the delivered energy.

Fig. 4 – Continuous IPW curve trend calculated from the LVDTs' measurement over one second recording. IPW is presented as the average among all the samples pooled together plotted within the instantaneous minimum and maximum interval.

Fig. 5 – Boxplot showing IPW_{max} and IPW_{CT} divided by spinal level: T10; L1; L4.

Fig. 6 – Boxplot showing IPW_{max} and IPW_{CT} divided by group: HE and LE.

Table 1: Details of the donors together with details of each specimen.

Donor	Level	Age	Height (m)	BW (Kg)	Gender	BMD mgHA/cm3	Pedicle angle		CA_0	l_0
							Left (°)	Right (°)	(mm^2)	(mm)
A	T9-T10-T11	44	1.60	55	F	148.3	4.8	-0.5	174	31.5
A	T12-L1-L2	44	1.60	55	F	138.6	22.8	5.2	350	44.3
A	L3-L4-L5	44	1.60	55	F	100.5	6.1	17.1	461	51.1
B	T9-T10-T11	46	1.70	89.5	M	150.6	5.6	8.9	201	29.6
B	T12-L1-L2	46	1.70	89.5	M	156.2	16.1	8.8	360	44.6
B	L3-L4-L5	46	1.70	89.5	M	143.5	14.2	21.1	305	49.8
C	T9-T10-T11	56	1.73	70.0	M	128	12.3	10.7	203	35.6
C	T12-L1-L2	56	1.73	70.0	M	98.5	21.2	16.2	273	46.7
C	L3-L4-L5	56	1.73	70.0	M	111.0	19.5	19.9	246	53.0
D	T9-T10-T11	38	1.75	85.6	M	191.9	14.0	9.0	214	32.6
D	T12-L1-L2	38	1.75	85.6	M	184.5	14.5	20.2	314	44.6
D	L3-L4-L5	38	1.75	85.6	M	161.7	37.4	35.8	258	55.7
Median		45	1.72	77.8	-	145.9	14.3	13.4	266	44.6

Table 2: Details of the specimen following in vitro spinal burst fracture simulation. FR and LF indicate respectively the presence of fragment retropulsion and laminar fracture.

Donor	Level	Group	Energy (J)	Fracture type	FR	LF	CO (%)	IPW_{max} (%)	IPW_{res} (%)	IPW_{CT} (%)
A	T9-T10-T11	LE	148.0	A3.1.1	×	×	-0.7	15.7	2.8	1.9
A	T12-L1-L2	HE	182.0	A3.2.1	✓	✓	37.4	15.9	10.2	8.1
A	L3-L4-L5	LE	146.0	B2.3.1	×	×	18.4	9.9	-1.3	0.2
B	T9-T10-T11	HE	166.2	A3.3.3	✓	✓	9.7	40.7	8.1	4.7
B	T12-L1-L2	HE	200.6	A3.3.3	✓	✓	34.1	4.3	-	-1.1
B	L3-L4-L5	HE	218.5	A3.3.3	✓	✓	21.9	6.1	0.3	1.3
C	T9-T10-T11	LE	167.3	A3.2.1	×	×	5.4	18.9	11.5	8.1
C	T12-L1-L2	LE	146.6	A3.2.2	✓	✓	18.1	21.8	7.6	8.0
C	L3-L4-L5	HE	200.0	A3.3.3	✓	×	30.7	4.6	-0.3	0.1
D	T9-T10-T11	HE	223.8	A3.3.3	✓	✓	41.2	38.2	1.7	4.6
D	T12-L1-L2	LE	184.2	A3.3.3	✓	✓	51.5	20.3	7.0	4.8
D	L3-L4-L5	LE	183.5	A3.2.2	×	×	-9.0	6.9	-	5.5
Median		-	182.8	-	-	-	20.2	15.8	4.9	4.7

Figure 1

Click here to download high resolution image

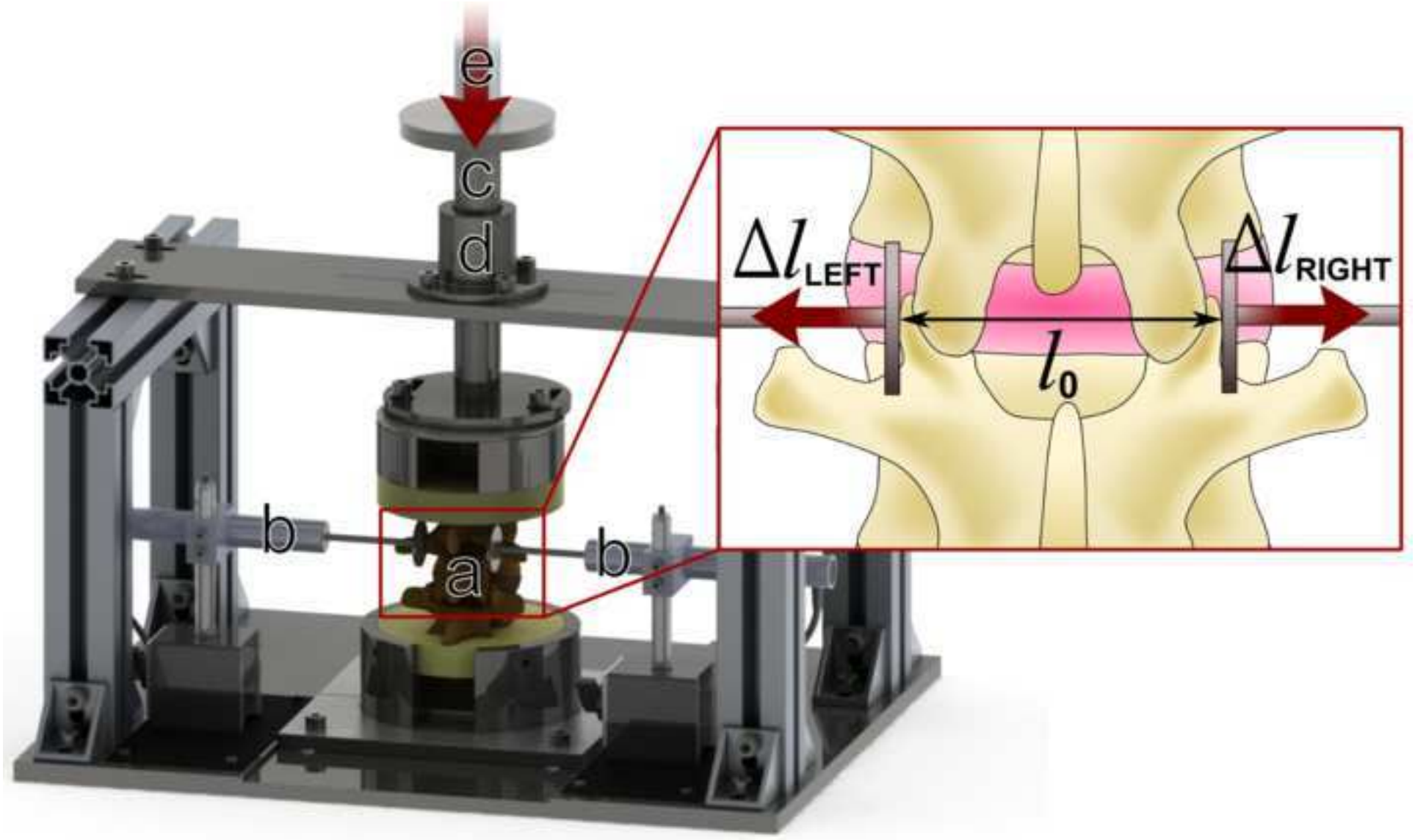

Figure 2

Click here to download high resolution image

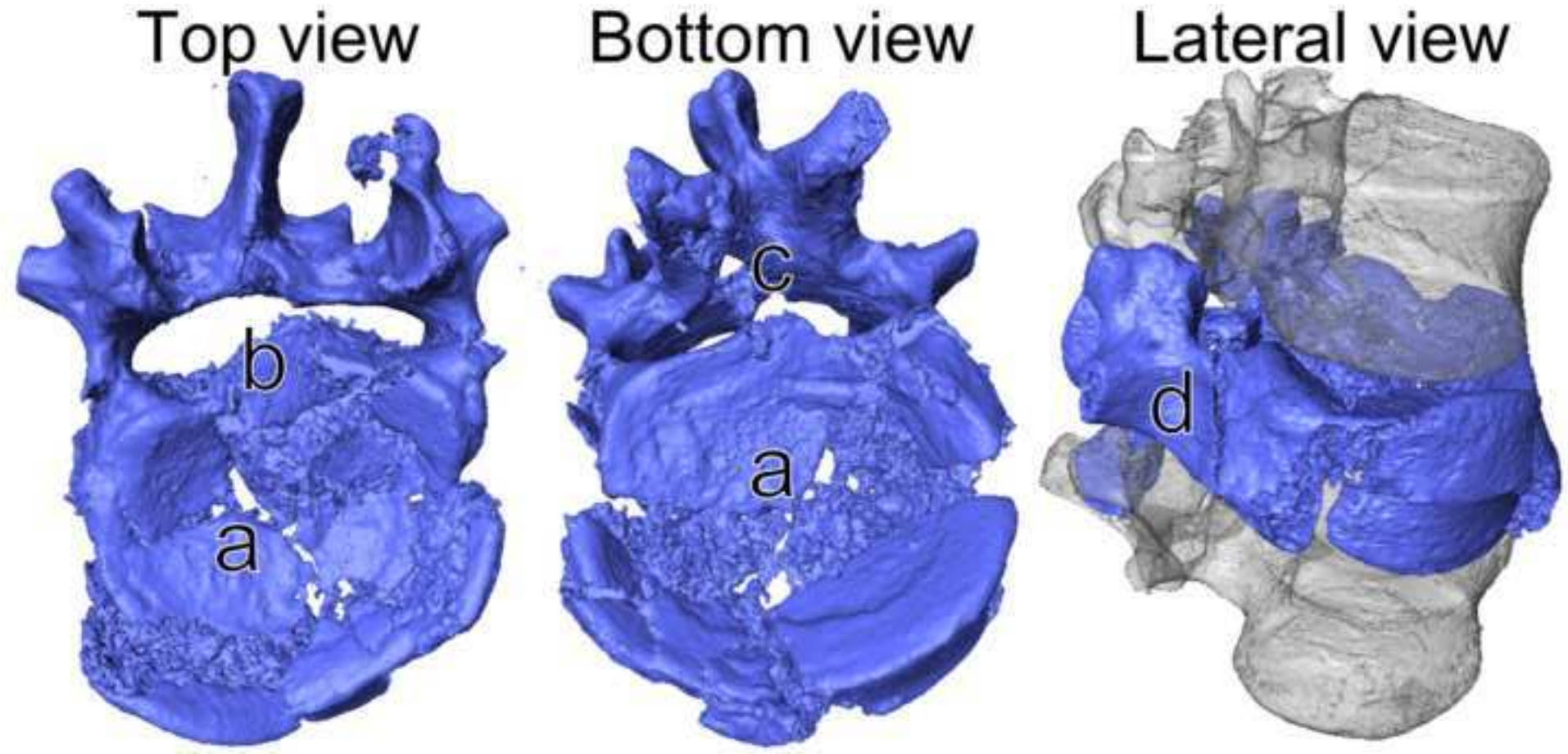

Figure 3

Click here to download high resolution image

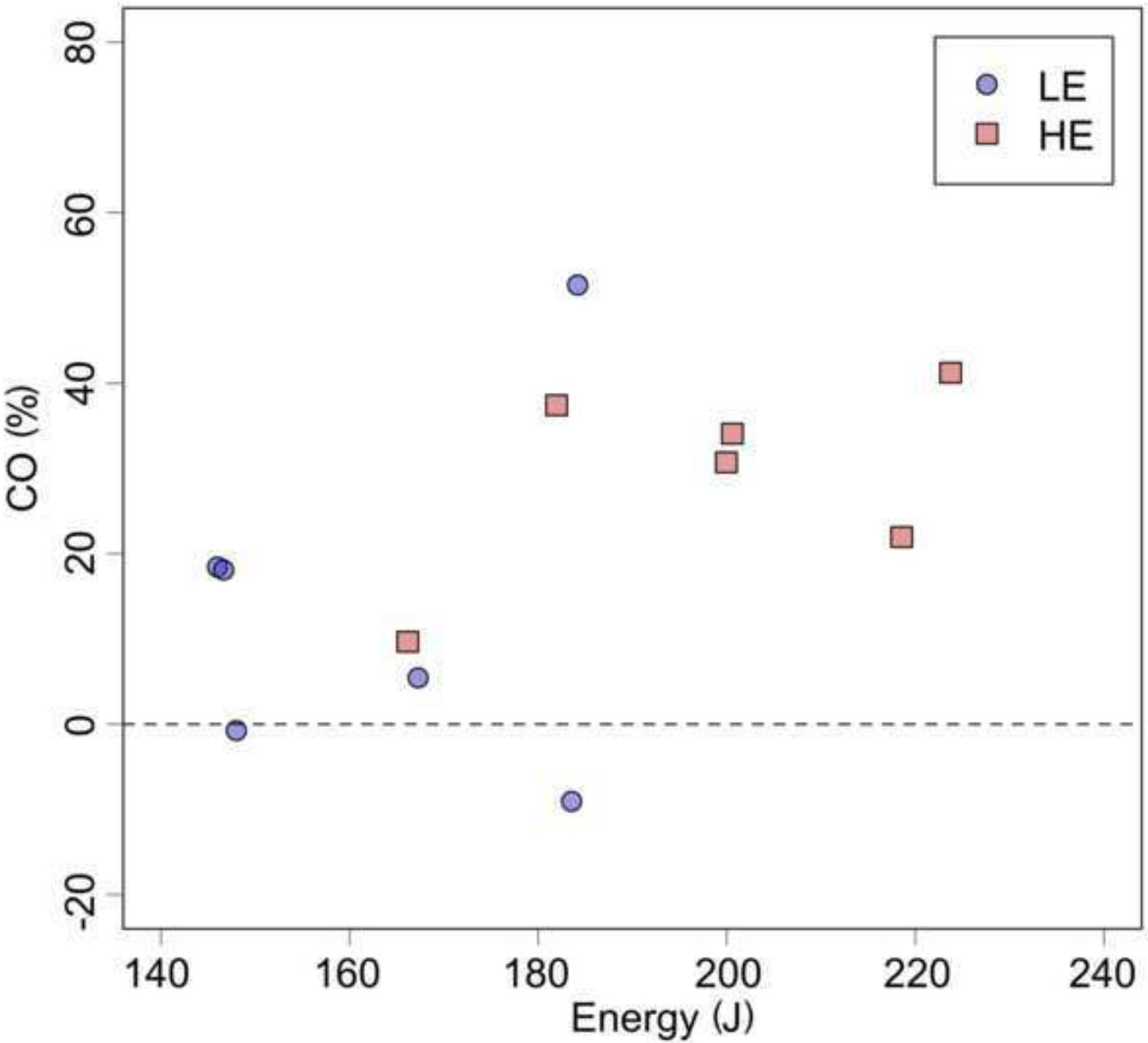

Figure 4

Click here to download high resolution image

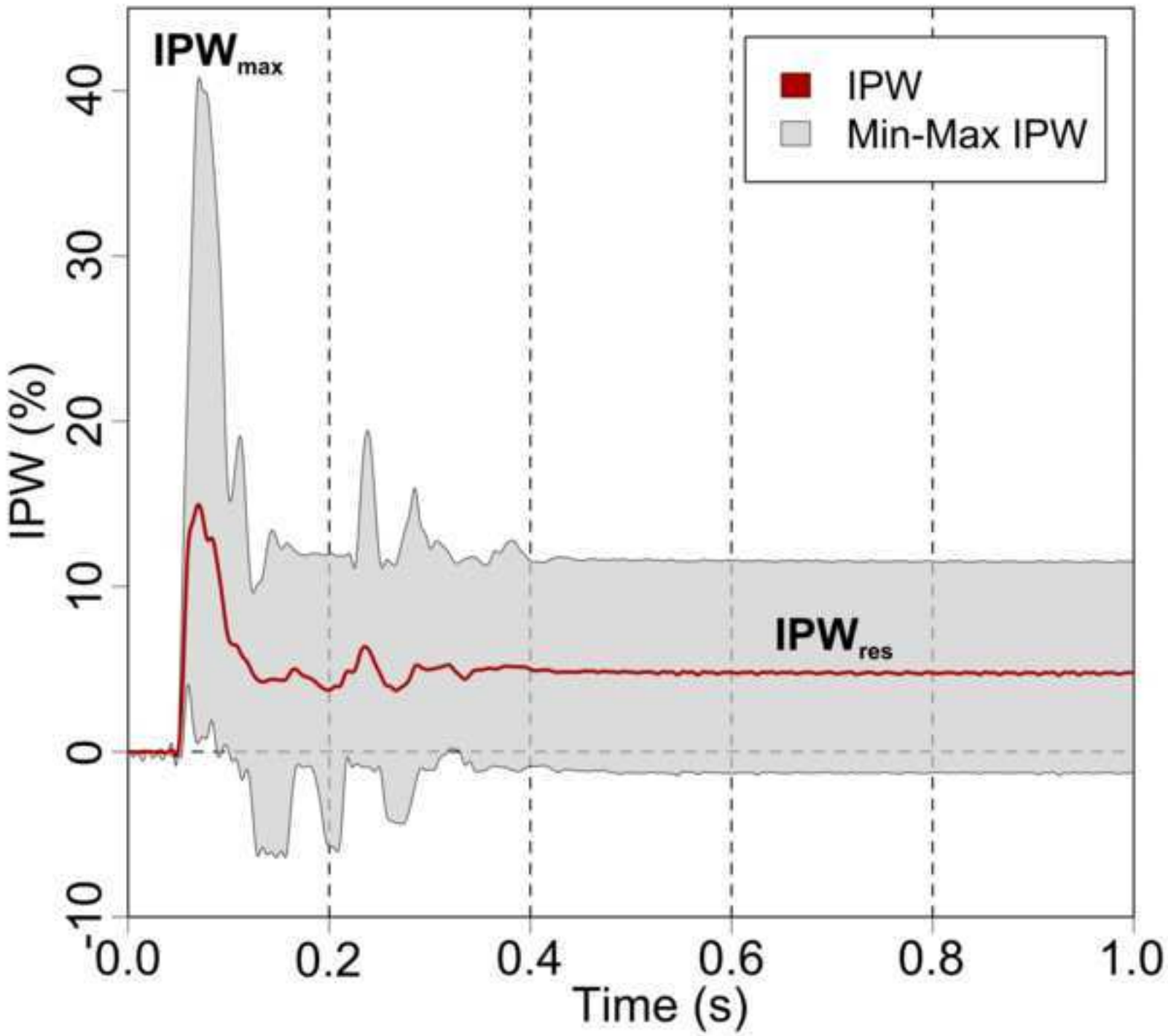

Figure 5

Click here to download high resolution image

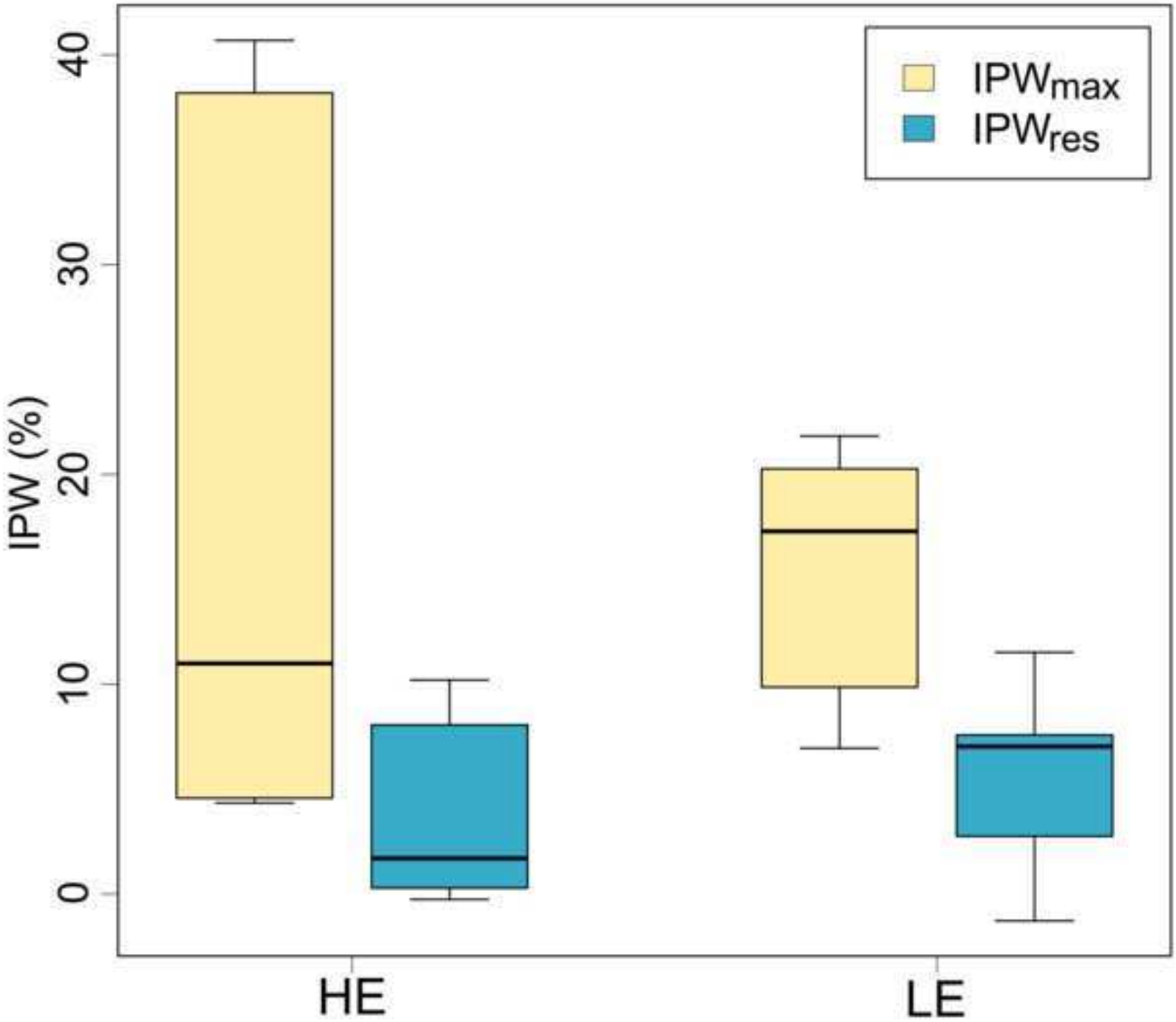

Figure 6

Click here to download high resolution image

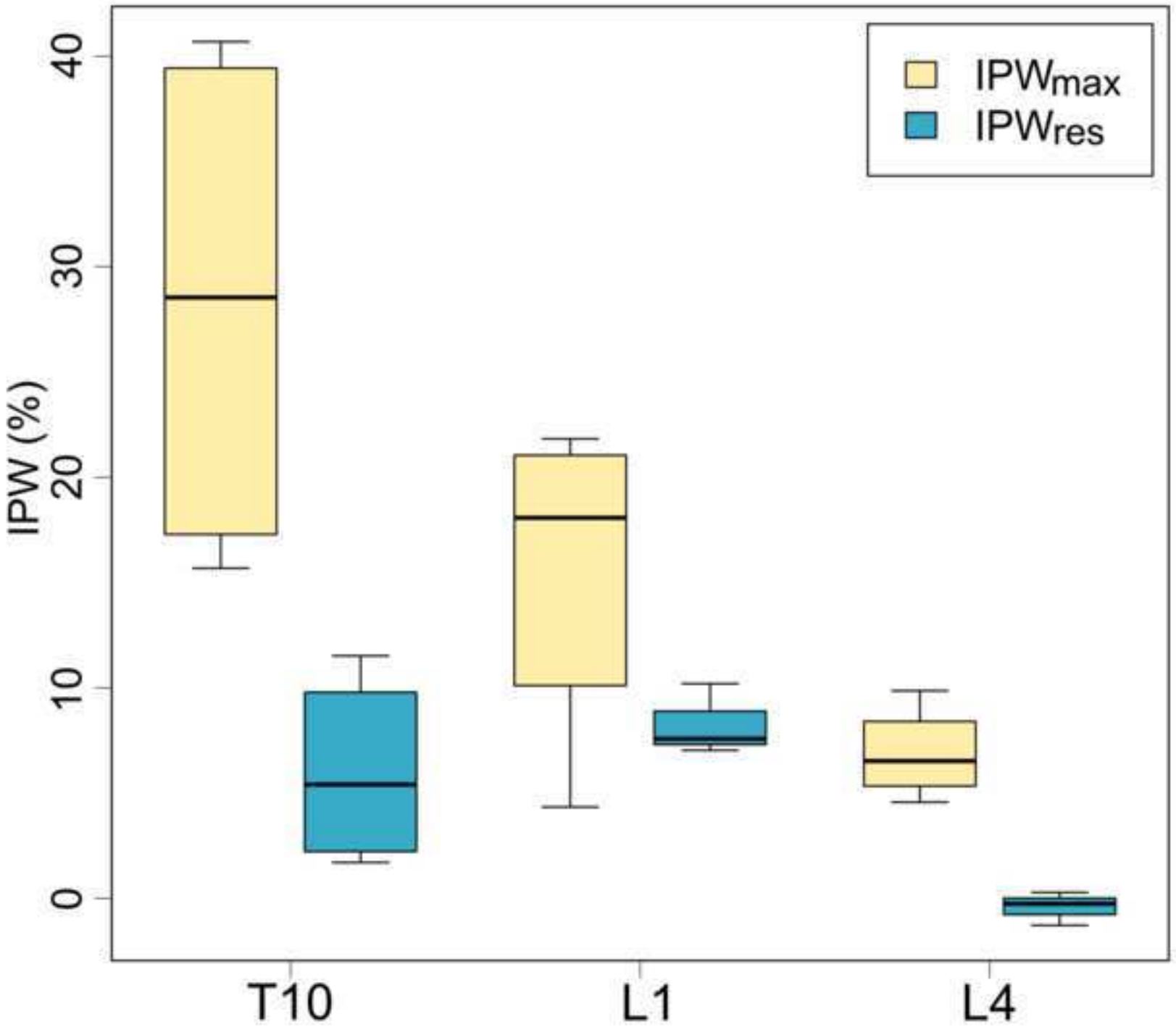

***Disclosure - Brandolini**

Click here to download Disclosure - TSJ-ICMJE Form: Author_Disclosure_Form_Brandolini.pdf

***Disclosure - Kapur**

Click here to download Disclosure - TSJ-ICMJE Form: Author_Disclosure_Form_Kapur.pdf

***Disclosure - Hall**

Click here to download Disclosure - TSJ-ICMJE Form: Author_Disclosure_Form_Hall.pdf

***Affirmation of Authorship Form**

Click here to download Affirmation of Authorship Form: Affirmation_Form.pdf

***FDA Drug/Device Approval Form**

Click here to download FDA Drug/Device Approval Form: FDA_Drug-Device_Disclosure.pdf